IJASRM
International Journal of Advanced Scientific Research and Management, Vol. 3 Issue 10, Oct 2018.
www.ijasrm.com
ISSN 2455-6378

Effect of Co^{2+} and Cr^{3+} Substituent's on Elastic Properties of Ni-Zn Ferrite

U. M. Mandle[1], L. A. Dhale[2], B. L. Shinde[3], K. S. Lohar[2*]

[1] Department of Chemistry, Sangmeshwar College,
Solapur, 413001 (M.S.) India

[2] Department of Chemistry, Shrikrishna Mahavidyalaya,
Gunjoti, 413606, Dist: Osmanabad (M.S.) India

[3] Department of Chemistry, Waghire College,
Saswad, Dist: Pune, 412301 (M.S.) India

Abstract

Co^{2+} and Cr^{3+} substituted $Ni_{0.5}Co_xZn_{0.5-x}Fe_{2-y}Cr_yO_4$ (x = y = 0.1 0.2, 0.3, 0.4, and 0.5) ferrites were prepared by sol-gel auto-combustion method. The prepared samples were sintered at 600 ^{0}C for 4 hours. The sintered samples were characterized by EDAX, XRD and I.R Spectroscopic method. The XRD patterns illustrate the single phase cubic structure. The lattice constant (a) decreases with increase of Co^{2+} and Cr^{3+} contents. The Infrared spectra were recorded within the range of 300-800 cm^{-1}. The two major bands observed, higher frequency band 'υ_1' (568 - 587 $cm^{-1)}$ assigned to tetrahedral sites, while lower frequency band 'υ_2' (422 - 447 $cm^{-1)}$ is assigned to octahedral site. The elastic properties such as Young modulus, Bulk modulus, Rigidity modulus, Poisson's ratio, and Debye temperature were calculated by using structural and IR data. The elastic moduli and Debye temperature increases with the Co^{2+} and Cr^{3+} contents.

***Keyword**: Ferrite, Infrared spectra, Elastic properties, Debye temperature*.

1. Introduction

Ni-Zn ferrite is soft magnetic material (Gabal M. A. et al. 2015, Gheisari K. et al. 2013, Han Q. J. et al. 2012) recently studies in electronic devices, because of its high resistivity, low eddy current loses, high Curie temperature, mechanical hardness, chemical stability (Ateia E. E. et al. 2014, Kumar K. V. & Ravinder D. 2002). IR spectroscopy is the most powerful techniques, to identify the structure of the molecule rapidly. Various bands obtained in the IR spectrum to corresponding the characteristic functional group and bond position in the chemical substance (Waldron R. D. 1955). The tetrahedral [A] and octahedral [B] sites of the spinel structure identify the absorption bands of the IR spectra (Patange S. M., Jadhav S. P. et al. 2013). The elastic properties of the ferrites study the behaviour of the solid is important to understand the nature of the bonding forces such as inter atomic and inter ionic bonding (Shirsath S. E. et al. 2012, Bhatu S. S. et al. 2007). The synthesis of the ferrite by various methods hydrothermal (Li X. & Wang G. 2009), wet chemical (Bharti D. C. 2010), co-precipitation (Amiri S. 2013), sol gel (Yue Z. et al. 2004), among these methods sol-gel method is low cost, better homogeneity, low temperature.

The elastic properties such as Young modulus, Bulk modulus, Rigidity modulus, Poisson's ratio, and Debye temperature were calculated by using structural and IR data (Modi K. B. et al. 2013, Patange S. M.; Lohar K. S. et al. 2013, Algude S. G. et al. 2014). The effect of Co^{2+} and Cr^{3+} on Elastic Properties of $Ni_{0.5}Co_xZn_{0.5-x}Fe_{2-y}Cr_yO_4$ (x = y = 0.1 0.2, 0.3, 0.4, and 0.5) ferrites prepared by sol-gel auto-combustion method were studied.

2. Materials and Methods

Nano crystalline $Ni_{0.5}Co_xZn_{0.5-x}Fe_{2-y}Cr_yO_4$ (x = y = 0.0, 0.1, 0.2, 0.3, 0.4, and 0.5) were synthesized by the sol-gel auto-combustion method. (Yue Z. et al. 2004) Analytical reagent grade all nitrate were dissolved in distilled water to obtain a mixed solution. The reaction procedure was carried out in an air atmosphere without the protection of inert gases. The molar ratio of metal nitrates to citric acid was 1:3. The brown-coloured ashes formed referred

IJASRM
International Journal of Advanced Scientific Research and Management, Vol. 3 Issue 10, Oct 2018.
www.ijasrm.com
ISSN 2455-6378

to as the precursor. The precursors were sintered at 600 ^{0}C for 4 hours.

The sintered samples were characterized, XRD examined by Phillips X-ray diffractometer (Model 3710) using Cu-K_α radiation (λ=1.5405Å). The morphology of the sample was studied by scanning electron microscopy. The composition was determined by energy dispersive X-ray spectroscopy (EDAX, Inca Oxford, attached to the SEM). The infrared spectra of all the samples were recorded at room temperature in the range 200 cm^{-1} to 800 cm^{-1} using the Perkin Elmer infrared spectrophotometer.

3. Results and Discussion

3.1. Chemical composition and Morphology:

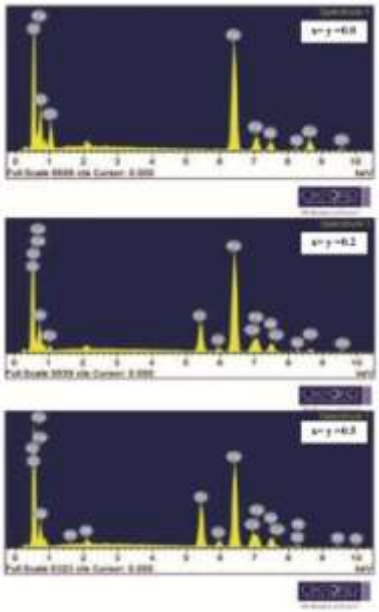

Fig. 1. Energy-dispersive X-ray spectroscopy Patterns x = y = 0.0, 0.2 and 0.5.

Energy dispersive X-ray spectroscopy (EDAX) analyses were carried out to determine the elemental stoichiometric composition of the sample to support our observations on the structure of the Ni-Zn ferrite with $Co^{2+}$and Cr^{+3}substitutions. EDAX patterns of typical samples are shown in Fig. 1. (x = y = 0.0, 0.3, and 0.5). The observed elemental analysis from EDAX is in good agreement with the theoretical composition used for the synthesis.

The morphology of the sample was studied by scanning electron microscopy. (SEM) The typical SEM images for (x= y = 0.0, 0.5) sample is shown in the fig. 2. It can be seen from fig.2. The fine crystals showed the tendency agglomeration. This agglomeration indicates that the prepared samples are high reactivity (Patange S. M.; Lohar K. S. et al 2013).

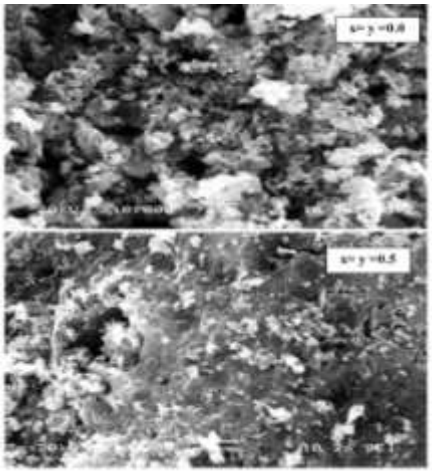

Fig.2. Scanning electron microscopy (SEM) image of the typical sample (x = y=0.0, and 0.5)

3.2. XRD:

The typical XRD patterns of sample (x = y= 0.0, and 0.5) shown in fig 3. The XRD patterns single phase cubic structure without other impurity phases. The lattice constant 'a' calculated by using equation (Cullity B. D. 2001) tabulated in table no. 1. The lattice constant is decreases from 8.360 **Å** to 8.298 **Å** with the increase in Co^{2+} and Cr^{3+} ions substitution to the Ni-Zn ferrite system.

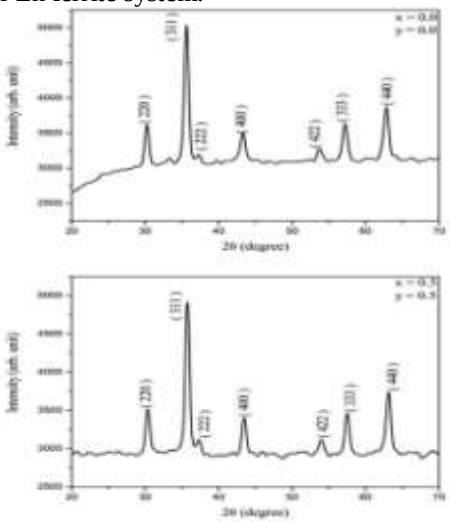

Fig. 3: Typical XRD patterns of Ni0.5CoxZn0.5-xFe2-y CryO4 (x = y = 0.0 and 0.5)

The decrease in lattice constant is related to ionic radii of respective ions, the substitution of the smaller Co^{2+} (0.065 nm) ions for the larger Zn^{2+} (0.074 nm) ions (Mohit K. et al. 2014, Kadam R. H. et al. 2013). At the same related to the ionic radii of the respective ions. In the present ferrite system smaller Cr^{3+} (0.63nm) ionic radii replace larger ions with Fe^{3+} (0.67 nm) ionic radii. Similar variations for

IJASRM
International Journal of Advanced Scientific Research and Management, Vol. 3 Issue 10, Oct 2018.
www.ijasrm.com
ISSN 2455-6378

Cr^{3+} ions are observed. The lattice constant (a) and cell volume (Vcell) are decreased slightly with the increase in dopant (Co-Cr) contents (Javed I. M. et al. 2012), Vegard's law (Vegard L. 1921).
The X-ray density 'd_x' was calculated by using the following relation,

$$d_x = \frac{nM}{N_A V} \quad (1)$$

Where,
d_x = X-ray density
n = Number of molecules per unit volume (8 for cubic structure)
M = Molecular weight of the composition
N_A = Avogadro's number = 6.02214×10^{23}
V = Volume = a^3
The values of X-ray density are presented in the table 1. X-ray density decreases with increasing Co^{2+} and Cr^{3+} content x from 5.404 to 5.376 g/cm^3.

Table 1: Lattice constant (a), X-ray Density (dx), Band Position (υ_1 and υ_1)

Comp x and y	'a'	'dx'	Band position	
			υ_1 cm^{-1}	υ_2 cm^{-1}
0.0	8.360	5.404	568.103	422.834
0.1	8.353	5.394	567.836	423.100
0.2	8.342	5.392	576.632	427.632
0.3	8.333	5.387	580.097	424.700
0.4	8.323	5.383	583.362	436.694
0.5	8.298	5.376	587.027	446.823

3.3. Infra-red spectroscopy:

IR spectra of the Co^{+2} and Cr^{+3} substituted Ni–Zn ferrites, recorded at room temperature in the frequency range 300–800 cm^{-1}, shown in Fig. 4.

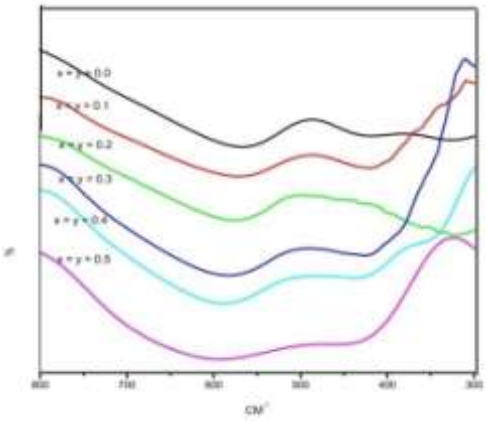

Fig.4. Infra red spectrum of Ni0.5CoxZn0.5-xFe2-y CryO4 (x=y = 0.00-0.5).

The bands' positions at different Cr-content were summarized in the table 1. The higher frequency band υ_1 tetrahedral (568.103-588.027 cm^{-1}) and lower frequency band υ_2 Octahedral (425.834-501.823 cm^{-1}) are assigned. The according to the Waldron (Waldron R. D. 1955), the higher vibration of the tetrahedral sites compared with that of octahedral sites can be due to the shorter bond length of the tetrahedral cluster and the long bond length of the octahedral cluster. The result showed that the sudden increase in the tetrahedral and octahedral sites with increases in the Co^{2+} and Cr^{3+} ions. Due to increases in the band position can be attributed in the accordance with the calculated ionic radii are R_A and R_B (table 2).

Table 2: Bond length, Force constants and Mean Force constant

Comp x and y	Bond length		Force constant (dyne/cm)		Mean Force constant
	R_A(Å)	R_B(Å)	K_0 x 10^5	K_t x 10^5	(K)
0.0	0.3856	0.3062	1.347	1.124	1.236
0.1	0.3848	0.3059	1.456	1.167	1.311
0.2	0.3840	0.3057	1.477	1.208	1.342
0.3	0.3832	0.3054	1.481	1.267	1.374
0.4	0.3829	0.3053	1.491	1.308	1.400
0.5	0.3819	0.3049	1.571	1.551	1.561

The variation in the cation-oxygen bond length in the lattice of the spinel. The displacement of the fe^{3+} by $Cr^{3+}$and Zn^{2+} by Co^{2+} ions. That decreases in the metal oxygen bond length and consequently increasing frequency. The similar reported in the literature. (Gabal M. A. et al. 2013). The bond lengths R_A and R_B calculated using the formula Gorter (Gorter E. W. 1954) are found to decrease with Co and Cr content x (Table 2). The decrease in bond lengths is attributed to the decrease in lattice constant (Patange S. M.; Lohar K. S. et al 2013). The IR spectra can give an idea about the molecular structure of the ferrites. The force constants corresponding to the tetrahedral and octahedral complexes are calculated by using the standard formulae given below

$$K_t = 7.62 \times M_1 \times \upsilon_1^2 \times 10^{-2} \quad (3)$$

$$K_o = 10.62 \times \frac{M_2}{2} \times \upsilon_2^2 \times 10^{-2} \quad (4)$$

where K_O is the force constant on octahedral site, K_t is the force constant on tetrahedral site, an M_1 molecular weight of tetrahedral site, an M_2 molecular weight of octahedral site, ν_1 the corresponding center frequency on tetrahedral site, and ν_2 the corresponding center frequency on octahedral site.

IJASRM
International Journal of Advanced Scientific Research and Management, Vol. 3 Issue 10, Oct 2018.
www.ijasrm.com
ISSN 2455-6378

The force constant is the second derivative of the potential energy with respect to the sight radius with the other independent parameters kept constant. the force constants K_t and K_O are listed in Table 2. The force constant K_t increases with the increasing Co^{2+} content whereas K_o increases with the increase in Cr^{3+}. This variation can be related to the difference in ionic radii of Zn^{2+} and fe^{3+} ions and their occupancy at A and B sites.

The average force constant (K) was calculated using following relation:

$$K=Kt+Ko/2 \quad (5)$$

The average force constant is increases with the Co^{2+} and Cr^{3+} ions.

Analysis of IR spectra with crystallographic knowledge helps us to determine the Debye temperature and elastic properties. The Debye temperature (θ_l) of all samples was calculated using the wave number of IR bands (Mazen S. A. et al. 2007),

$$\theta l=\hbar C\upsilon_{ac}/\kappa \quad (6)$$

Where, ħ = h/2p, k is Boltzmann constant, C is the velocity of light (C = $3x10^8$ cm/s) and υ_{av} is average wave number of bands. Debye temperature (θ_l) with the Co^{2+} content x is shown in the fig.5. The Debye temperature increased with increased in the Co^{2+} andCr^{3+}.

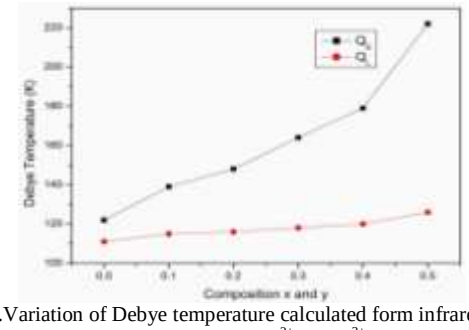

Fig.5.Variation of Debye temperature calculated form infrared (θI) and elastic (θ_E) data with $Co^{2+}$and Cr^{3+}content..

3.4. Elastic properties:

In general, there are 36 elastic moduli, among the three elastic modulis reduced in the spinel ferrite. For the spinel ferrite system, elastic constant and the Debye temperature can be calculated using IR data using the relation discussed elsewhere (Modi K. B. 2013, Patange S. M.; Lohar K. S. et al 2013) .

The stiffness constant (C_{11} and C_{12}) was calculated using the following relation (Patange S. M.; Lohar K. S. et al 2013):

$$C_{11}=\frac{K}{a} \quad (7)$$

$$(C_{12})=\frac{\sigma \quad C_{11}}{(1-\sigma)} \quad (8)$$

where K is the average force constant and a is the lattice constant. The values of Poisson's ratio (s) were calculated using the relation discussed elsewhere (Algude S. G. et al. 2014) and the values are presented in Table 3. Using equation 7 and 8 the stiffness constant is calculated and the values tabulated in table 3.

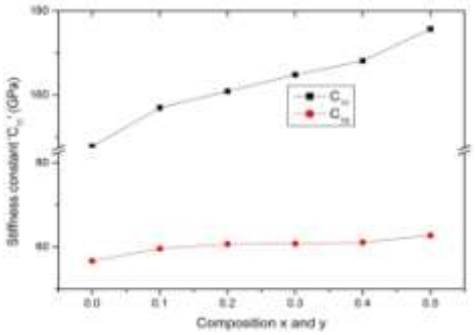

Fig. 6. Variation of stiffness constants (C_{11} and C_{12}) with $Co^{2+}$and Cr^{3+}content.

It is observed from fig.6 both the stiffness constant increased with increase in Co^{2+} and Cr^{3+} substitution. The stiffness constant values affected by the strong bonding between the atoms and force constant. The values of Poisson's ratio show the nonlinear behavior in the range of 0.277–0.263, this value lies in the range from 1to 0.5 which is in conformity with the theory of elasticity (Patil V. G. et al. 2009).

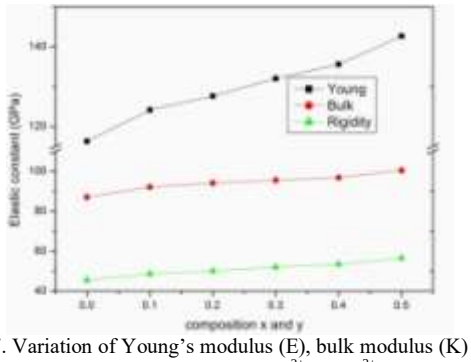

Fig. 7. Variation of Young's modulus (E), bulk modulus (K) and modulus of rigidity (G) with $Co^{2+}$and Cr^{3+}content

The elastic moduli's are calculated using relation (Modi K. B. et al. 2013). The Rigidity modulus (G), Bulk Modulus (B) and young modulus(E) increases with an increase in both Co^{2+} its shown in fig .7. which indicates that easy deformation in the solid and it has less tendency to spring back to its equilibrium position.

IJASRM International Journal of Advanced Scientific Research and Management, Vol. 3 Issue 10, Oct 2018.
www.ijasrm.com
ISSN 2455-6378

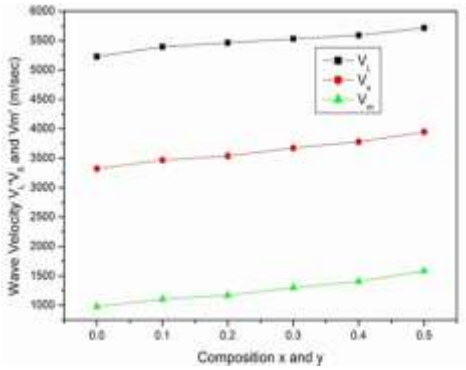

Fig. 8. Variation of shearing velocity (VS), mean wave velocity (Vm) and longitudinal wave velocity (VL) with $Co^{2+}$and Cr^{3+}content.

According to Wooster (Wooster W. A. 1953) work the increases in the modulus attributed interatomic bonding between Co, Zn, Ni, Fe, Cr ions in present ferrite composition. The interatomic bonding between ions weakens continuously with the substitution of the Co^{2+} ions, therefore, increases in modulus with increasing Co^{2+} content (Algude S. G. et al. 2014).The elastic wave velocities such as Longitudinal wave velocity (V_L), transverse (shear) wave velocity (VS) and average wave velocity(V_M) calculated by relation (Patange S. M.; Lohar K. S. et al 2013).

Table 3: Pore Fraction, Possion's ratio σ, $C_{11,}C_{12,}$ elastic modulli

Comp. x and y	Pore Fraction	Possion's ratio σ	C_{11}	C_{12}	Youngs modulus	Bulk modulus	Rigdity modulus
0.0	0.138	0.277	147.81	56.73	116.34	87.09	45.54
0.1	0.144	0.275	156.99	59.65	124.15	92.10	48.67
0.2	0.148	0.274	160.92	60.73	127.64	94.12	50.09
0.3	0.161	0.270	164.85	60.85	132.04	95.51	52.00
0.4	0.170	0.267	168.17	61.12	135.59	96.80	53.53
0.5	0.180	0.263	186.92	66.76	151.78	106.81	60.08

It is illustrated from fig 8, the values of V_L, V_S, and V_M increased with an increase in the $Co^{2+}$and Cr^{3+} content (Algude S. G. et al. 2014). The average velocity increases the inter atomic bond strength increases between the Fe^{3+} and Cr^{3+} ions.

Debye temperature(θ_E) was calculated using formula (Anderson O. L. 1965),

$$\theta_E = \frac{h}{k}\left[\frac{3\rho q N_A}{4\Pi M}\right]^{1/3} \times V_m \qquad (9)$$

The variation of Debye temperature (θ_E) is given in fig 5. The Debye temperature increased with increase in substitution of the Co^{2+} and Cr^{3+} ions.

6. Conclusions

The Co^{2+} and Cr^{3+} substituted Ni-Zn ferrite synthesized by the Sol gel auto combustion method. The observed elemental analysis from EDAX is in good agreement with the theoretical composition used for the synthesis. The XRD patterns confirm the single phase cubic structure. The frequency bands of the 'υ_1' and 'υ'_2 both increased with increase in Co^{2+} and Cr^{3+} contents. The elastic moduli and Debye temperature increases with the Co^{2+} and Cr^{3+} contents.

References

[1] Algude, S. G., Patange, S. M., Shirsath, S. E., Mane, D. R., & Jadhav, K. M. Elastic behaviour of Cr3+ substituted Co–Zn ferrites. *Journal of Magnetism and Magnetic Materials*, *350*, 39-41 (2014).

[2] Amiri, S., & Shokrollahi, H. Magnetic and structural properties of RE doped Co-ferrite (REåNd, Eu, and Gd) nano-particles synthesized by co-precipitation. *Journal of Magnetism and Magnetic Materials*, *345*, 18-23 (2013).

[3] Ateia, E. E., Ahmed, M. A., Salah, L. M., & El-Gamal, A. A. Effect of rare earth oxides and La3+ ion concentration on some properties of Ni–Zn ferrites. *Physica B: Condensed Matter*, *445*, 60-67 (2014).

[4] Bharti, D. C., Mukherjee, K., & Majumder, S. B. Wet chemical synthesis and gas sensing properties of magnesium zinc ferrite nano-particles. *Materials Chemistry and physics*, *120*(2-3), 509-517 (2010).

[5] Bhatu, S. S., Lakhani, V. K., Tanna, A. R., Vasoya, N. H., Buch, J. U., Sharma, P. U., ... & Modi, K. B. Effect of nickel substitution on structural, infrared and elastic properties of lithium ferrite (2007).

[6] Cullity, B. D. Chemical analysis by X-ray diffraction. *Elements of X-ray diffraction, Addison-Wesley, Massachusetts*, 397-420 (2001).

[7] Gabal, M. A., Bayoumy, W. A., Saeed, A., & Al Angari, Y. M. Structural and

electromagnetic characterization of Cr-substituted Ni–Zn ferrites synthesized via Egg-white route. *Journal of Molecular Structure*, *1097*, 45-51 (2015).

[8] Gabal, M. A., Al Angari, Y. M., & Al-Agel, F. A. Synthesis, characterization and magnetic properties of Cr-substituted Co–Zn ferrites nanopowders. *Journal of Molecular Structure*, *1035*, 341-347 (2013).

[9] Gheisari, K., Shahriari, S., & Javadpour, S. Structure and magnetic properties of ball-mill prepared nanocrystalline Ni–Zn ferrite powders at elevated temperatures. *Journal of Alloys and Compounds*, *552*, 146-151 (2013).

[10] Gorter, Evert Willem. Philips Res. Rep. 9, 295-320 (1954)

[11] Han, Q. J., Ji, D. H., Tang, G. D., Li, Z. Z., Hou, X., Qi, W. H., ... & Bian, R. R. Estimating the cation distributions in the spinel ferrites Cu0. 5− xNi0. 5ZnxFe2O4 (0.0≤ x≤ 0.5). *Journal of Magnetism and Magnetic Materials*, *324*(12), 1975-1981 (2012).

[12] Javed Iqbal, M., Ahmad, Z., Meydan, T., & Melikhov, Y. Physical, electrical and magnetic properties of nano-sized Co-Cr substituted magnesium ferrites. *Journal of applied physics*, *111*(3), 033906 (2012).

[13] Kadam, R. H., Birajdar, A. P., Alone, S. T., & Shirsath, S. E. Fabrication of Co0. 5Ni0. 5CrxFe2− xO4 materials via sol–gel method and their characterizations. *Journal of Magnetism and Magnetic Materials*, *327*, 167-171 (2013).

[14] Kumar, K. V., & Ravinder, D. Electrical conductivity of Ni–Zn–Gd ferrites. *Materials letters*, *52*(3), 166-168 (2002).

[15] Li, X., & Wang, G. Low-temperature synthesis and growth of superparamagnetic Zn0. 5Ni0. 5Fe2O4 nanosized particles. *Journal of Magnetism and Magnetic Materials*, *321*(9), 1276-1279 (2009).

[16] Mazen, S. A., Zaki, H. M., & Mansour, S. F. Infrared absorption and dielectric properties of Mg–Zn ferrite. *International Journal of pure and applied physics*, *3*(1), 40-48 (2007).

[17] Modi, K. B., Shah, S. J., Pujara, N. B., Pathak, T. K., Vasoya, N. H., & Jhala, I. G. Infrared spectral evolution, elastic, optical and thermodynamic properties study on mechanically milled Ni0. 5Zn0. 5Fe2O4 spinel ferrite. *Journal of Molecular Structure*, *1049*, 250-262 (2013).

[18] Mohit, K., Gupta, V. R., Gupta, N., & Rout, S. K. Structural and microwave characterization of Ni0. 2CoxZn0. 8− xFe2O4 for antenna applications. *Ceramics International*, *40*(1), 1575-1586 (2014).

[19] O.L. Anderson, W.P. Mason (Eds.), Physical Acoustics, vol. 3B, Academic Press, New York, p. 43-95 (1965).

[20] Patange, S. M., Shirsath, S. E., Jadhav, S. P., Hogade, V. S., Kamble, S. R., & Jadhav, K. M. Elastic properties of nanocrystalline aluminum substituted nickel ferrites prepared by co-precipitation method. *Journal of Molecular Structure*, *1038*, 40-44 (2013).

[21] Patange, S. M., Shirsath, S. E., Lohar, K. S., Algude, S. G., Kamble, S. R., Kulkarni, N., & Jadhav, K. M. Infrared spectral and elastic moduli study of NiFe2− xCrxO4 nanocrystalline ferrites. *Journal of Magnetism and Magnetic Materials*, *325*, 107-111 (2013).

[22] Patil V. G., Shrisath Sagar E., More S. D., Shukla S. J., Jadhav K. M J. Effect of zinc substitution on structural and elastic properties of cobalt ferrite, *Alloys Compd.* 488,199-203 *(*2009).

[23] Shirsath, S. E., Patange, S. M., Kadam, R. H., Mane, M. L., & Jadhav, K. M. Structure refinement, cation site location, spectral and elastic properties of Zn2+ substituted NiFe2O4. *Journal of molecular structure*, *1024*, 77-83 (2012).

[24] Vegard, L. The constitution of mixed crystals and the space occupied by atoms. *Z. Phys*, *5*(17), 17-26 (1921).

[25] Waldron, R. D. Infrared spectra of ferrites. *Physical review*, *99*(6), 1727 (1955).

[26] Wooster, W. A. Physical properties and atomic arrangements in crystals. *Reports on Progress in Physics*, *16*(1), 62 (1953).

[27] Yue, Z., Guo, W., Zhou, J., Gui, Z., & Li, L. Synthesis of nanocrystilline ferrites by sol–gel combustion process: the influence of pH value of solution. *Journal of magnetism and magnetic materials*, *270*(1-2), 216-223 (2004).